Two Functionally Distinct NADP$^+$-Dependent Ferredoxin Oxidoreductases Maintain the Primary Redox Balance of *Pyrococcus furiosus*

Diep M. N. Nguyen[1], Gerrit J. Schut[1], Oleg A. Zadvornyy[2], Monika Tokmina-Lukaszewska[3], Saroj Poudel[4], Gina L. Lipscomb[1], Leslie A. Adams[1], Jessica T. Dinsmore[1], William J. Nixon[1], Eric S. Boyd[4], Brian Bothner[3], John W. Peters[2] and Michael W. W. Adams[1]*

[1]Department of Biochemistry and Molecular Biology, University of Georgia, Athens, GA 30602, USA

[2]Institute of Biological Chemistry, Washington State University, Pullman, WA 99164

[3]Department of Chemistry and Biochemistry, Montana State University, Bozeman, MT 59717

[4]Department of Microbiology and Immunology, Montana State University, Bozeman, MT 59717

Running title: Functions of Two Nfns in *Pyrococcus furiosus*

*To whom correspondence should be addressed: Department of Biochemistry and Molecular Biology University of Georgia, Athens, GA 30602-7229 Tel: 706 542-2060. FAX: 706 542-0229 E-mail: adamsm@uga.edu

Keywords: Archaea; Hyperthermophile; Electron bifurcation; Nfn; Metabolism; sulfur

SUPPLEMENTAL MATERIALS

Tables S1 – S4 and Figures S1 – S11

Table S1. Primers designed and used recombinant strains in this study

Primers	Sequence
DN.039	CTAGGTCTATCTTCCTCC CTT C
DN.040	GGTGTTCCTCAAACATTTTCAAGTATGCACATCACCCTACAAG
DN.041	ATCCATCGGGCAATTCATGG
DN.042	GATTATTGGGAGGTGGAGAAAAATGCATCACCACCATCACCA
	CCACCATCACGGTTATAAAATCCTCGAGAAAAAGGAAATCG
DN.043	CTCTTTTACAACTTCAAATACCTG
DN.044	GTTCCTCAAACATTTTCAAGGATGAACACCTCCGATCACG
DN.045	CTTTACCCATTCAACAATCTTCTCTG
DN.053	CTAGGTCTATCTTCCTCCCTTC
DN.060	GAT TAT TGG GAG GTG GAG AAA AAT GCA TCA CCA CCA TCA CCA CCA CCA
	TCA CGG TTT CAA AAT TTT AAG AAA AGA GAG GC
DN.073	GGGAAGCCGCTAAGAAGATTTTC
DN.074	CGAAAATCTTCTTAGCGGCTTCCCTTAAATTAACATCTTTATTTTTTCAAG G
DN.075	CGAAAATCTTCTTAGCGGCTTCCCTATGCACATCACCCTACAAG
DN.076	GCTCTGCCCAATATGTCCACGCGGCCGCGTTTAAACGG
WN.017	CAGAGGCAAGTAACGAGAG
WN.018	GTGGACATATTGGGCAGAGCTGTTAGAACTAAACCTATTGAAATCGT
WN.019	GCTCTGCCCAATATGTCCACTTATCTTGAGCTCCATTCTTTCAC
WN.020	TGTTAGAACTAAACCTATTGAAATCGTTGGTCAAATGCTCATCATTTAGTTTTATG
WN.021	CAATAGGTTTAGTTCTAACAGCTCTGCCCAATATGTCCACTATGCACATCACCCT
	ACAAG
WN.022	AAA TCT GTC AAG CCT CGT GG
WN.023	GGTCTACTGGATTGGAACAG

WN.024	CACCTCTTTCTTATAACCTTTTTAGGAC
WN. 025	AAGGTTATAAGAAAGAGGTGTTATCTTGAGCTCCATTCTTTCAC
WN.026	CTTTTTAGGACGAAAGGTTTATATCTCCAGGATGTCAAATGCTCATCATTTAGTTTTATG
WN.027	ATATAAACCTTTCGTCCTAAAAAGGTTATAAGAAAGAGGTGGATGAACACCTCCGATCAC
WN.028	CACTTTCTCCTGGGAAACCAAC
SP2.088	CTTGAAAATGTTTGAGGAACACC
SP2.055	TTTTCTCCACCTCCCAATAATC

Table S2. Doubling times for growth of recombinant strains

Strains	**Doubling time (T_D)**		
	M	**MS**	**PS**
COM1c	1.06	1.35	1.7
ΔNfnI	2.07	1.14	2.1
ΔNfnII	1.28	1.14	2.7
ΔNfnI- ΔNfnII	ND	ND	ND
OE-NfnI	1.5	1.1	3.4
OE-NfnII	3.1	1.3	3.9

ND, not determined

OE, overexpression

Table S3. Nfn bifurcating activity detected in whole cell extracts

Strains	Nfn bifurcating activity (units mg^{-1})	
	M	**MS**
COM1c	0.13 ± 0.02	0.06 ± 0.02
ΔNfnI	<0.01**	<0.01**
ΔNfnII	0.11 ± 0.01	0.02 + 0.0

**Below detection limit

Standard deviations were derived from three technical measurements

Table S4. NfnII catalytic bias of FNOR activities

Electron donors	Electron acceptors	NfnII activity (units mg^{-1})
NADPH	Fd_{ox}	<0.01**
Fd_{red}*	$NADP^+$	12.2 ± 1.5

*Chemically reduced with Ti-citrate

**Below detection limit

Standard deviations were derived from three technical measurements

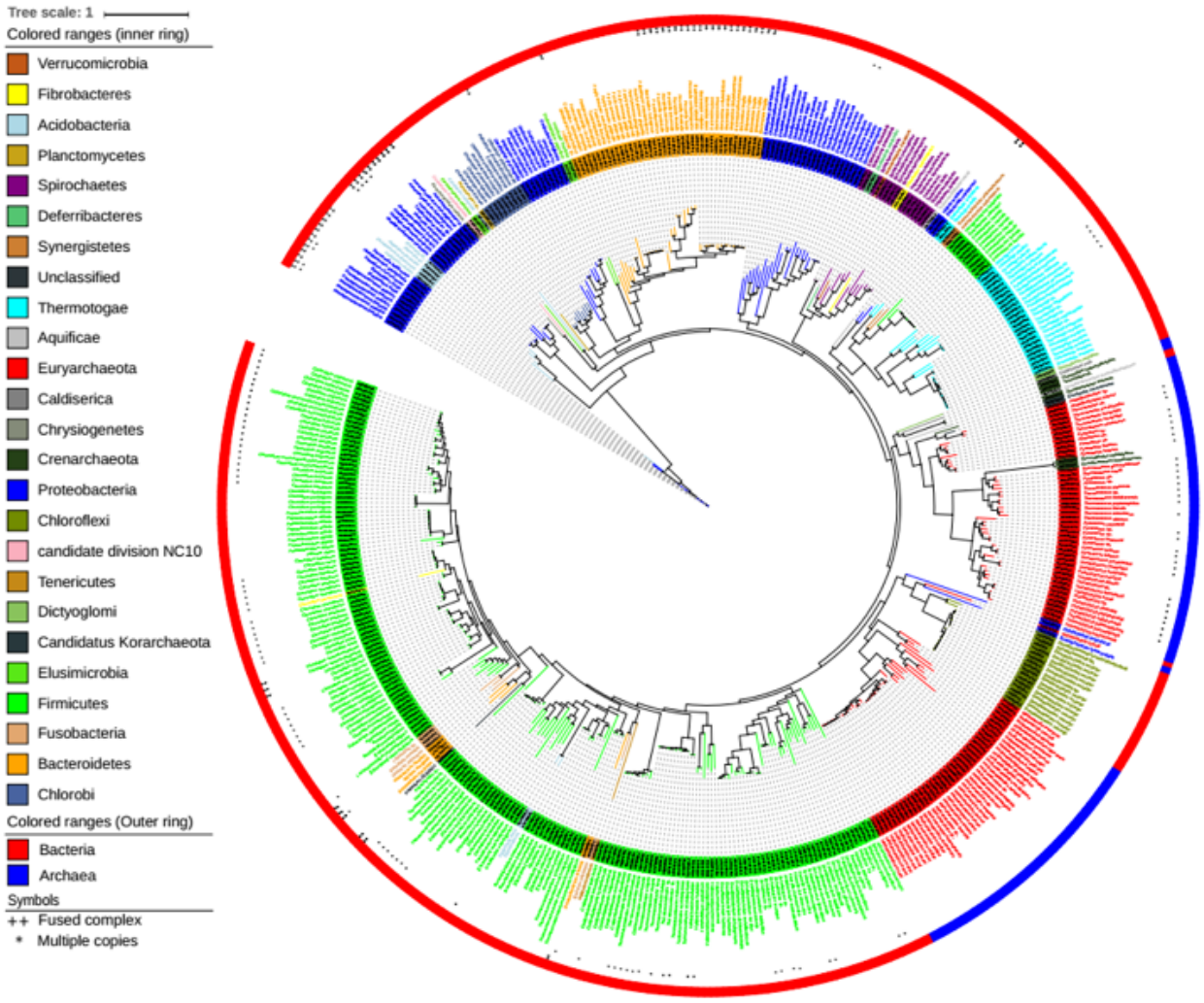

Figure S1. Phylogenetic reconstruction of a concatenation of 467 archaeal and bacterial NfnS and NfnL subunits. Phylum level taxonomic ranks were mapped onto the terminals of the tree. Double plus symbols (++) inside of the color ring denoting taxonomic ranks indicates that the subunits are fused, whereas an asterisk (*) denotes the presence of multiple copies of Nfn.

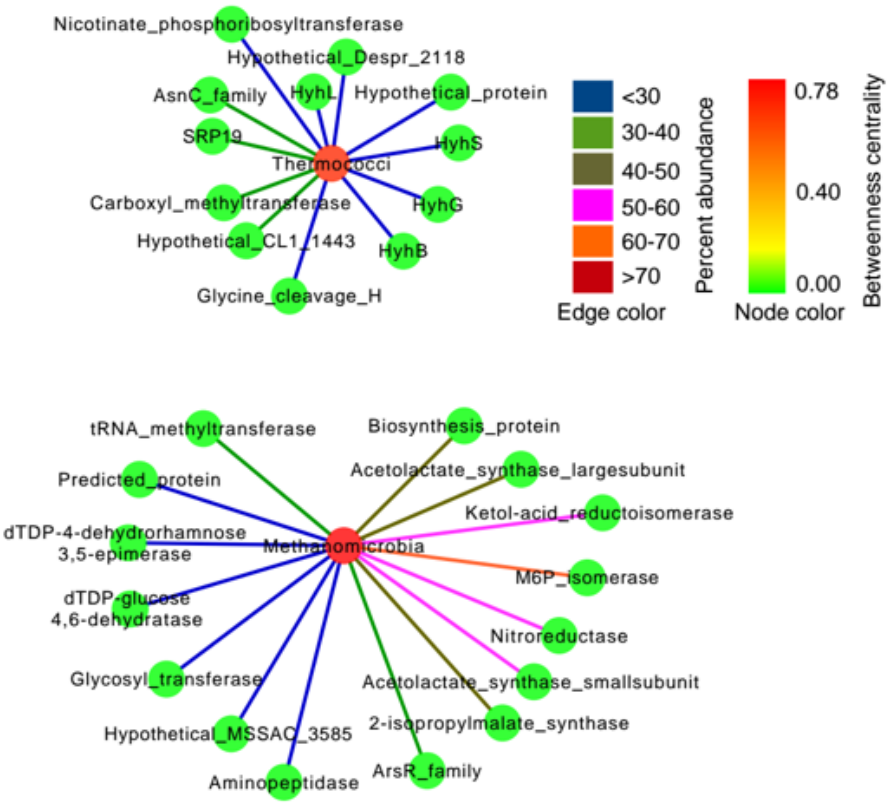

Figure S2. Network analysis of proteins encoded by genes flanking (+/-10) *nfnS*, as organized by the taxonomic rank of the genome where NfnS was recovered. Only proteins (n=29) that were identified in >20 % of the NfnSL encoding archaeal genomes were considered. Node color represents the betweenness centrality (a measure of the 'connectedness' of each gene) while the edge color represents the percent abundance.

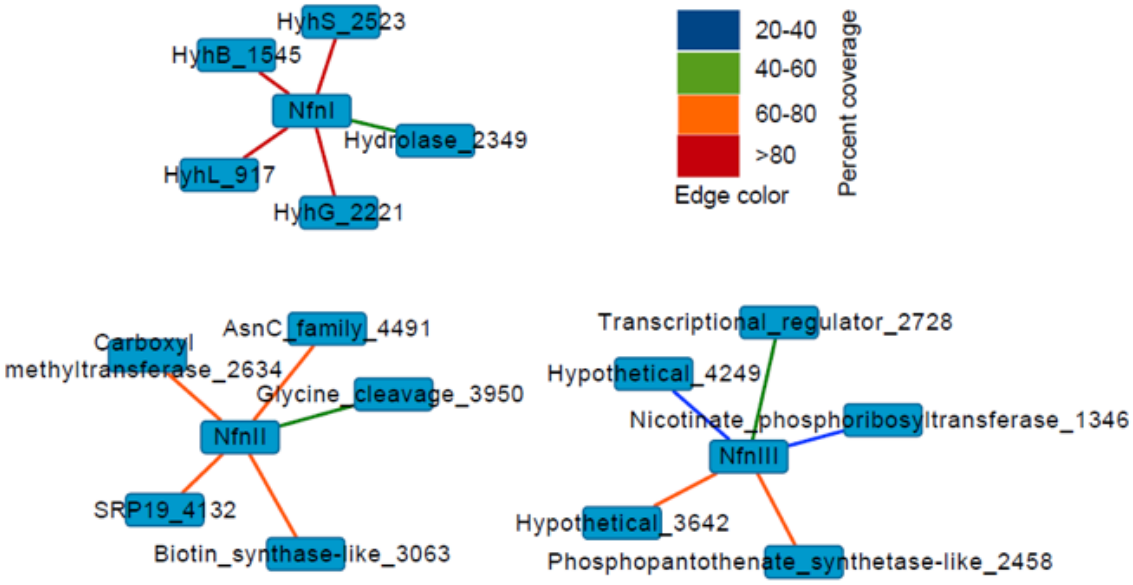

Figure S3. Network analysis of multiple isoforms of Nfn (i.e., NfnI, NfnII, and NfnIII) identified in archaeal genomes. Only proteins encoded in the flanking regions of >50 % of the each Nfn group (i.e. relative frequency of >50 %) for each individual Nfn were considered in this analysis. Here, the edge color represents the abundance of the protein (depicted as a node) in each group. The force directed organic layout was used to visualize the network.

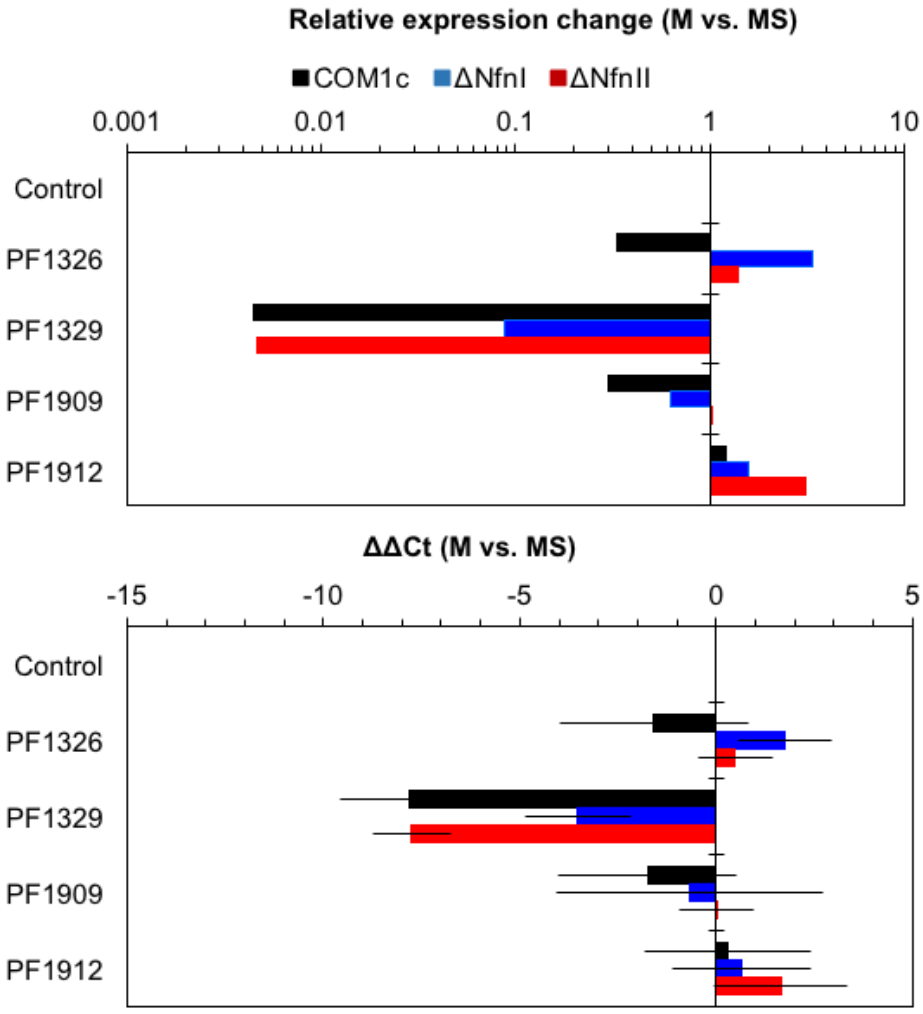

Figure S4. Expression change analysis of the up- and downstream genes of *nfnI* (PF1327-28) and *nfnII* (PF1910-11) genes in the ΔNfnI and ΔNfnII when using S^0 as terminal electron acceptor versus H^+ by RT-qPCR. The constitutively expressed DNA polymerase subunit gene PF0983, DNAp, was used as a control. PF1326, and PF1912 genes encoded for hypothetical genes. PF1329 encoded for the β-subunit of soluble hydrogenase II and PF1909 encoded for ferredoxin. The propagation errors were calculated from Ct values measured from cDNA that were derived from two biological samples. The top graph represents the fold changes in log based 10 scale and the bottom graph displays the observed ΔΔCt values.

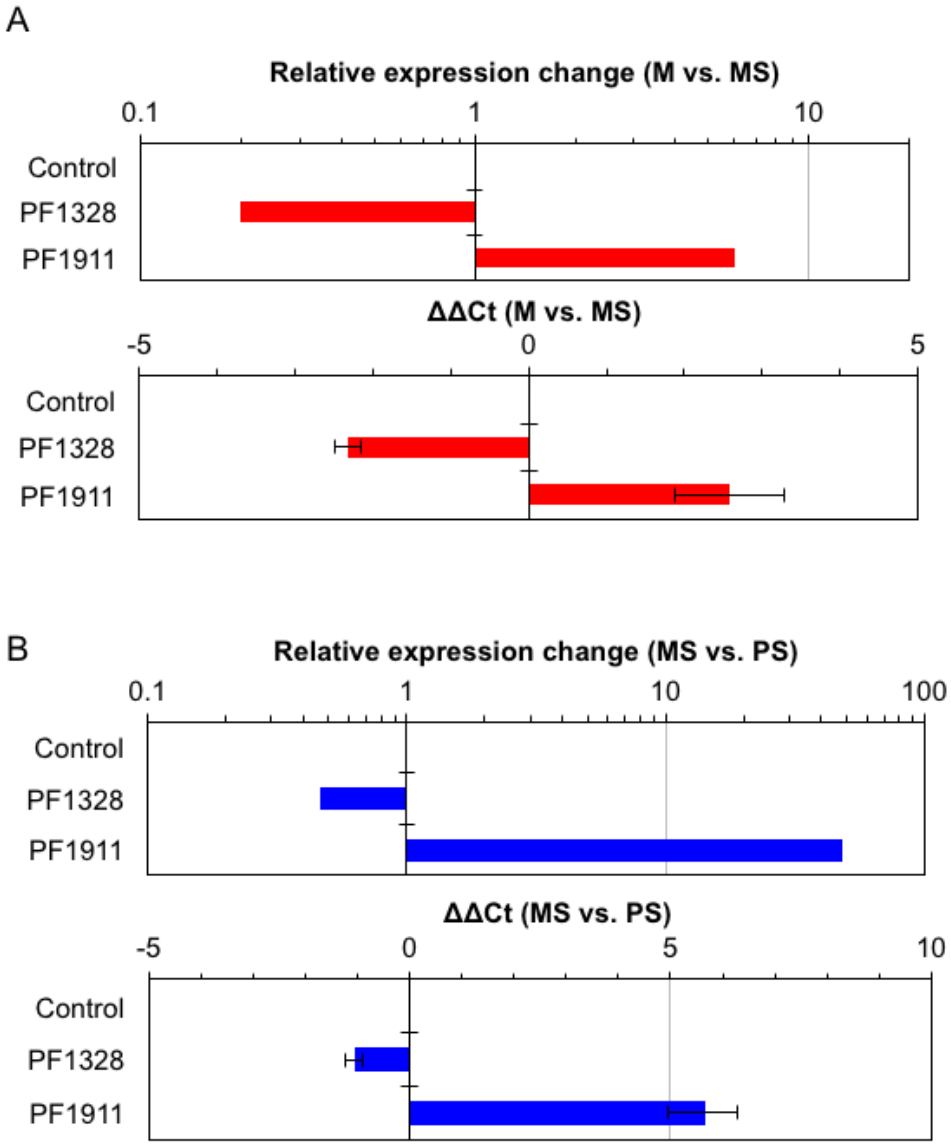

Figure S5. Expression change analysis of NfnI and NfnII when using S^0 as terminal electron acceptor versus H^+ (A) and when using peptides as the sole carbon source versus carbohydrates (B) by RT-qPCR. The constitutively expressed DNA polymerase subunit gene PF0983, DNAp, was used as a control. PF1328 and PF1911 genes encoded for NADH dependent ferredoxin NADP oxidoreductase I and II-small subunits (NfnI-S and NfnII-S, respectively). The propagation errors were calculated from Ct values measured from cDNA that were derived from two biological samples. The top graphs of (A) and (B)

represent the fold changes in log based 10 scale and the bottom graphs of (A) and (B) display the observed ΔΔCt values.

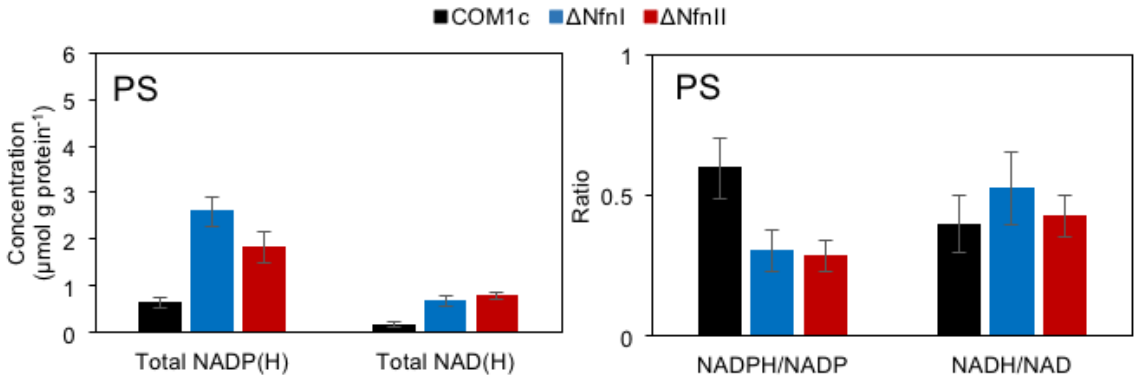

Figure S6. Redox nucleotide pool analysis: the total concentration of NADP(H), NAD(H), NADPH/NADP and NADH/NAD ratios of COM1c (black), ΔNfnI (blue), ΔNfnII (red) strains in PS medium at 90 ℃, 200 rpm. The standard deviations were derived from measurement taken from three independent biological samples.

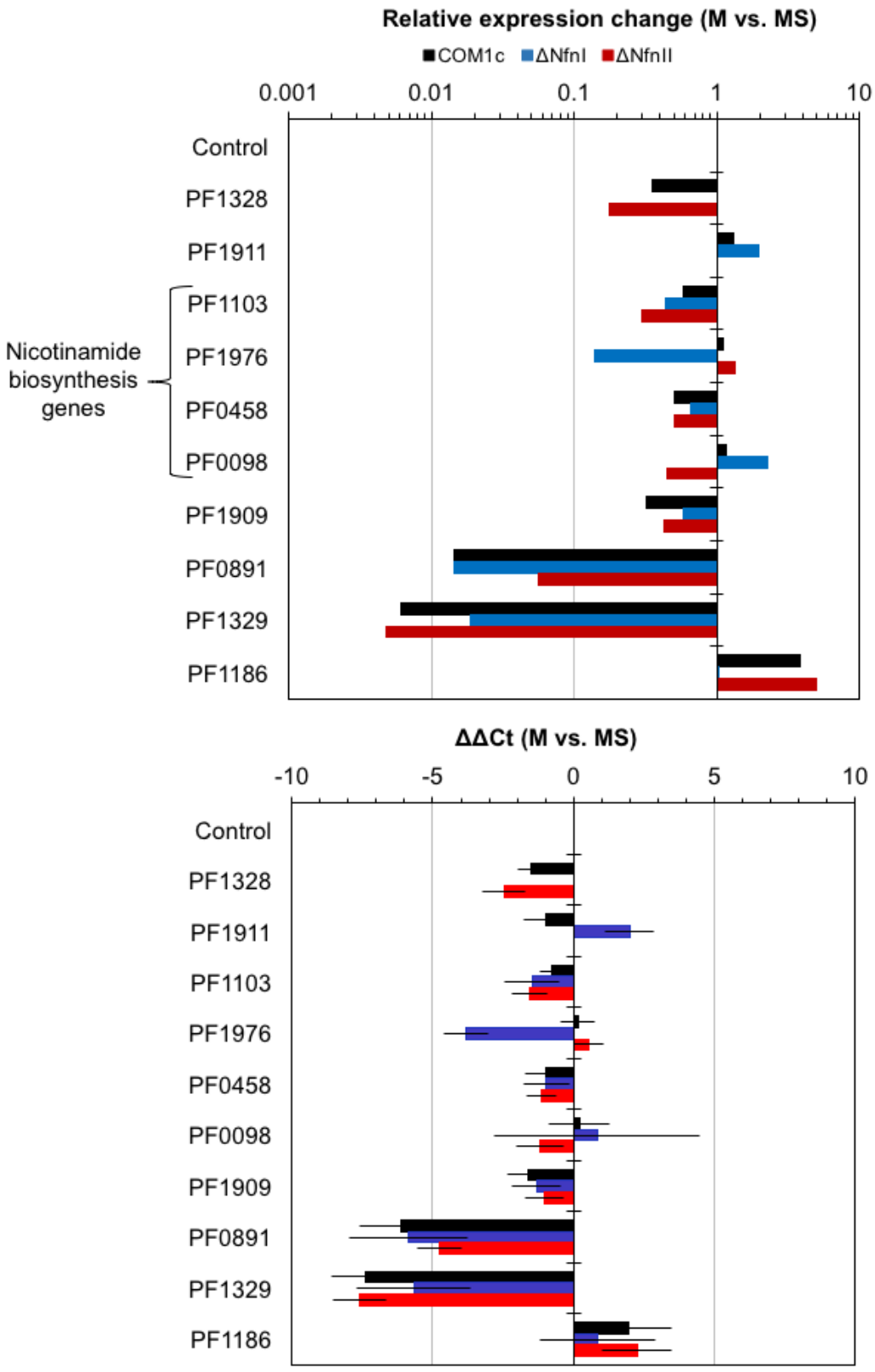
Relative expression change (M vs. MS)
COM1c
ΔNfnI
ΔNfnII
0.001
0.01
0.1
1
10
Control
PF1328
PF1911
PF1103
PF1976
PF0458
PF0098
PF1909
PF0891
PF1329
PF1186
Nicotinamide biosynthesis genes
ΔΔCt (M vs. MS)
-10
-5
0
5
10
Control
PF1328
PF1911
PF1103
PF1976
PF0458
PF0098
PF1909
PF0891
PF1329
PF1186

Figure S7. Expression change analysis of the control strain (black), ΔNfnI (blue) and ΔNfnII (red) trains when using S^0 as terminal electron acceptor versus H^+ (M versus MS media) by RT-qPCR. The constitutively expressed DNA polymerase subunit gene PF0983, DNAp, was used as a control. The following genes encoding proteins were analyzed: NADH dependent ferredoxin:NADP oxidoreductase I and II- small subunits (PF1328, NfnI-S, and PF1911, NfnII-S, respectively), NAD kinase (PF1103), L-asoartate oxidase (PF1976), NAD diphosphorylase (PF0458), NH_3-dependent NAD synthetase (PF0098), ferredoxin (PF1909), β-subunit of soluble hydrogenase I (PF0891) and II (PF1329) and NAD(P)H elemental sulfur oxidoreductase (PF1186, NSR). The propagation errors were calculated from Ct values measured from cDNA that were derived from two biological samples. The top graph represents the fold changes in log based 10 scale and the bottom graph displays the observed ΔΔCt values.

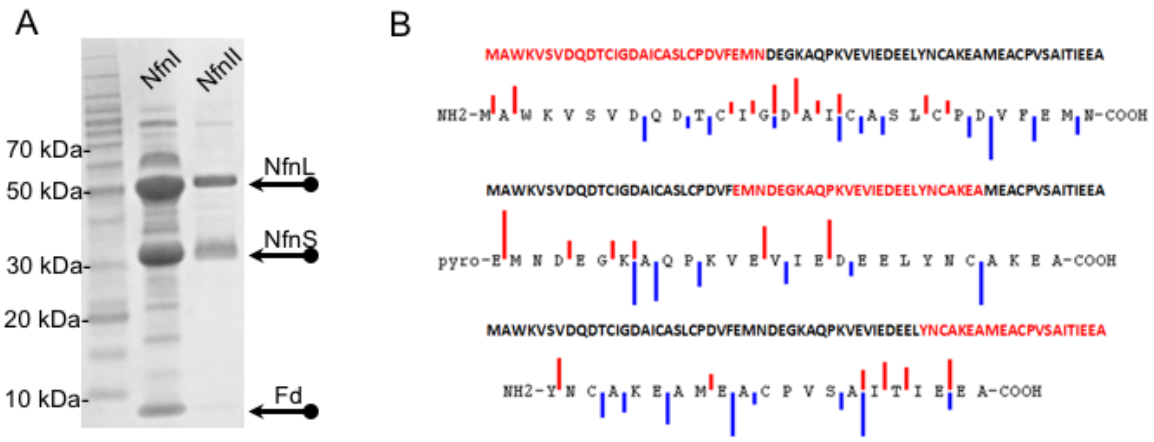

Figure S8. Identification of protein components in Nfn complexes. (A) SDS PAGE separation of purified complexes NfnI and NfnII. Protein bands indicated by the arrows were indentified as NfnI or NfnII small and large subunits in the course of tryptic digestion. (B) Three overlapping peptides from pepsin digestion used to identify ferredoxin (identified peptide is highlighted in red). Below the sequence is the MS/MS fragmentation matches, where red and blue lines represent b and y ions, respectively.

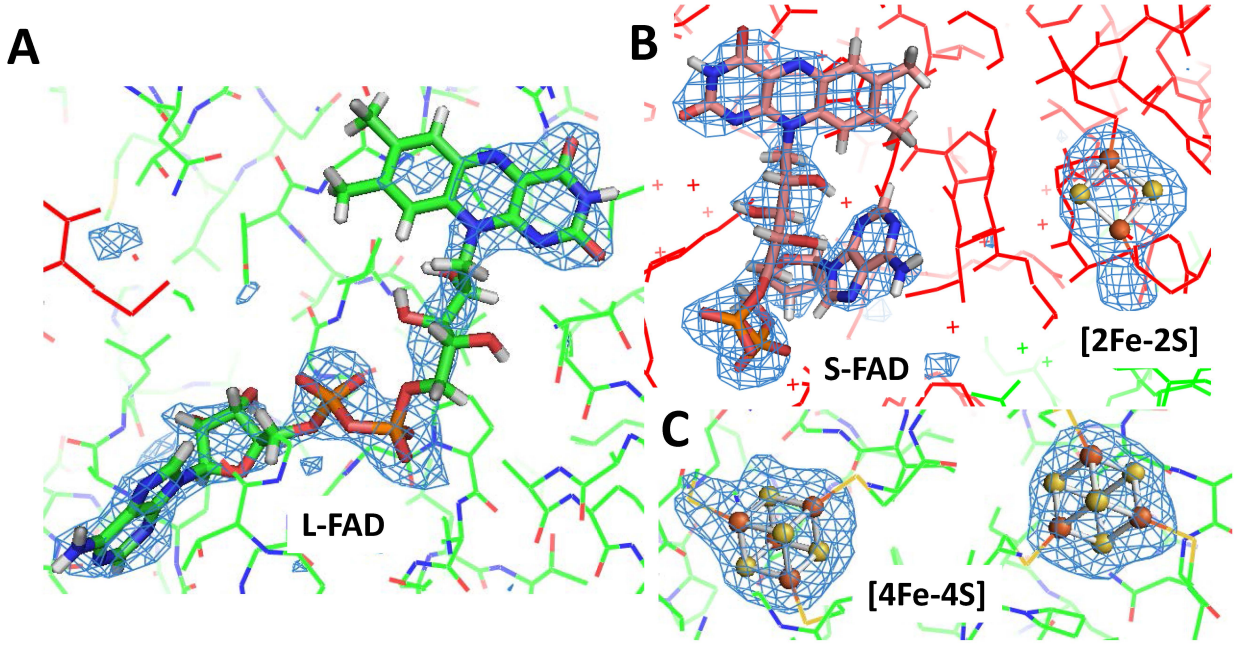

Figure S9. Structure of NfnII. The omit electron density map of NfnII contoured at 1.5 σ is shown in blue mesh calculated with omitted L-FAD (A), S-FAD and [2Fe-2S] cluster (B), and two [4Fe-4S] clusters (C). The NfnII-L subunit is colored in green and the NfnII-S subunit is colored in red. L-FAD and S-FAD are shown as sticks, and the FeS clusters as balls and sticks.

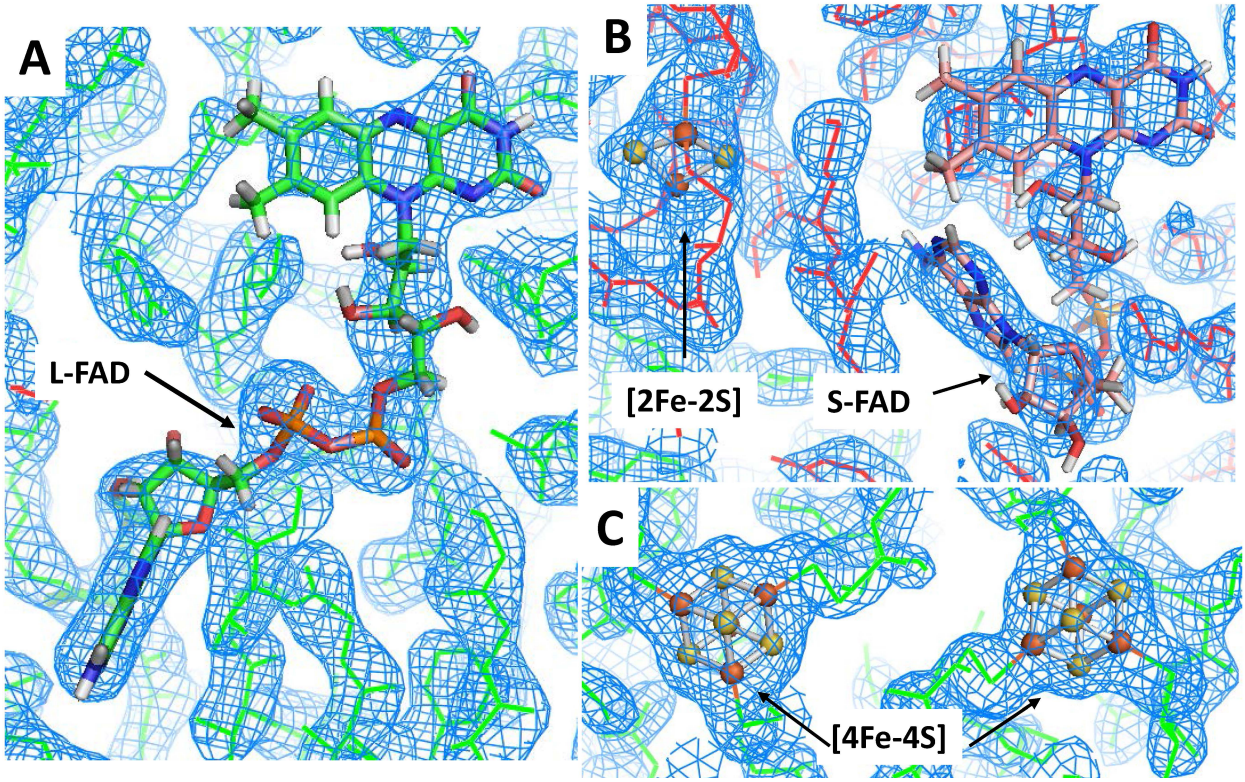

Figure S10. Structure of NfnII. The simple composite omit electron density map of NfnII contoured at 1.5 σ is shown in blue mesh around L-FAD (A), S-FAD and [2Fe-2S] cluster (B), and two [4Fe-4S] clusters (C). The NfnII-L subunit is colored in green and the NfnII-S subunit is colored in red. L-FAD and S-FAD are shown as sticks, and the FeS clusters as balls and sticks.

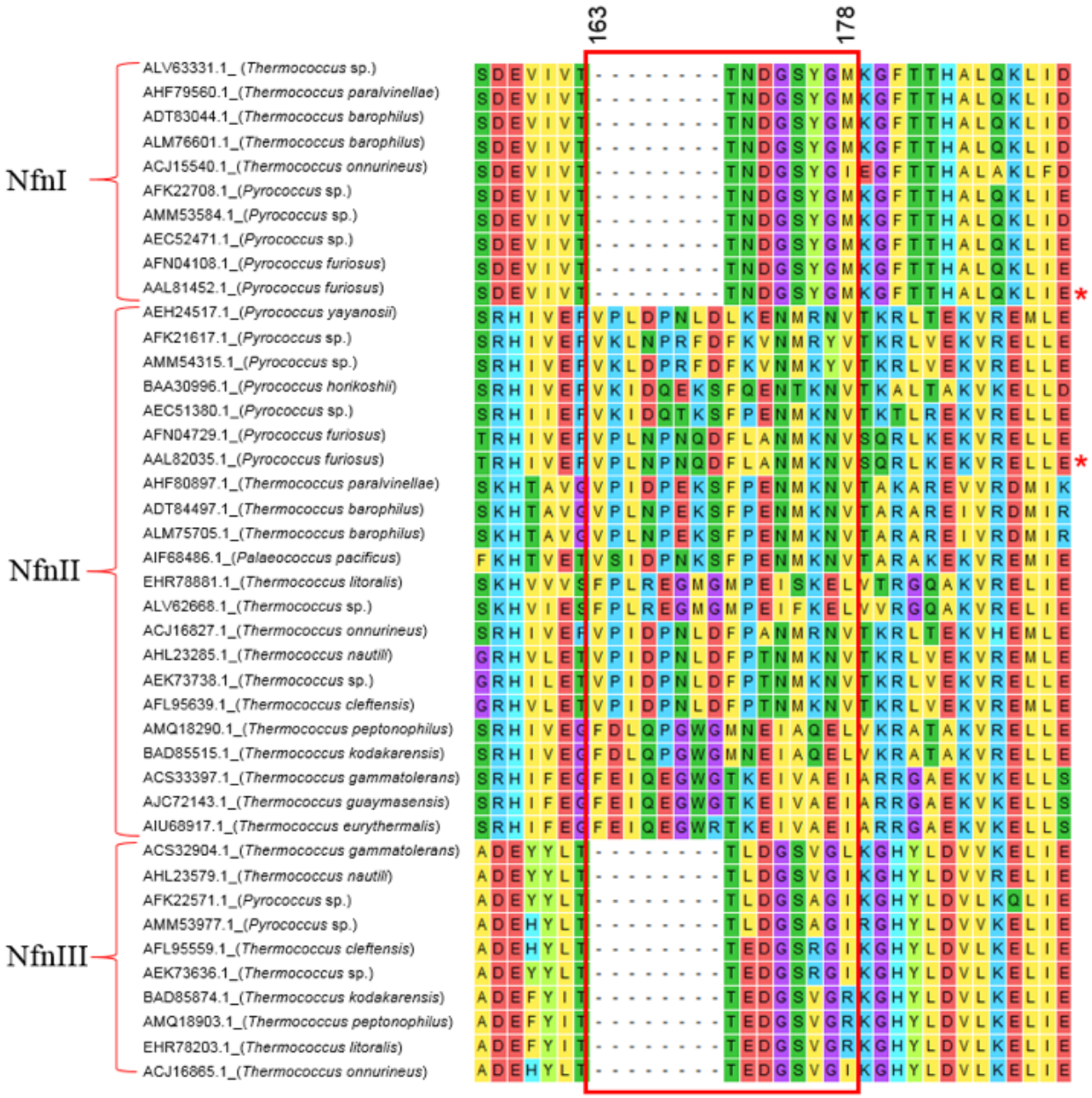

Figure S11. Multiple sequence alignment of a fragment of representative NfnI, NfnII and NfnIII protein sequences. Positions 163 to 178 are highlighted with a red box. The asterisk represents NfnI and NfnII from *P. furiosus* reported in this paper.